AGU PUBLICATIONS

Geophysical Research Letters

RESEARCH LETTER
10.1002/2016GL068424

Key Points:
- Mid-mantle seismic and gravity anomaly under Greenland identified
- Jurassic-Cretaceous slab linked to paleo-Arctic ocean closure, prior to Amerasia Basin opening
- Possible arc-mantle signature in Cretaceous High Arctic LIP volcanism

Supporting Information:
- Supporting Information S1

Correspondence to:
G. E. Shephard,
g.e.shephard@geo.uio.no

Citation:
Shephard, G. E., R. G. Trønnes, W. Spakman, I. Panet, and C. Gaina (2016), Evidence for slab material under Greenland and links to Cretaceous High Arctic magmatism, *Geophys. Res. Lett.*, *43*, 3717–3726, doi:10.1002/2016GL068424.

Received 13 OCT 2015
Accepted 18 APR 2016
Accepted article online 19 APR 2016
Published online 27 APR 2016

©2016. American Geophysical Union. All Rights Reserved.

Evidence for slab material under Greenland and links to Cretaceous High Arctic magmatism

G. E. Shephard[1], R. G. Trønnes[1,2], W. Spakman[1,3], I. Panet[4], and C. Gaina[1]

[1]Centre for Earth Evolution and Dynamics (CEED), Department of Geosciences, University of Oslo, Oslo, Norway, [2]Natural History Museum, University of Oslo, Oslo, Norway, [3]Department of Earth Sciences, Utrecht University, Utrecht, Netherlands, [4]Institut National de l'Information Géographique et Forestière, Laboratoire LAREG, Université Paris Diderot, Paris, France

Abstract Understanding the evolution of extinct ocean basins through time and space demands the integration of surface kinematics and mantle dynamics. We explore the existence, origin, and implications of a proposed oceanic slab burial ground under Greenland through a comparison of seismic tomography, slab sinking rates, regional plate reconstructions, and satellite-derived gravity gradients. Our preferred interpretation stipulates that anomalous, fast seismic velocities at 1000–1600 km depth imaged in independent global tomographic models, coupled with gravity gradient perturbations, represent paleo-Arctic oceanic slabs that subducted in the Mesozoic. We suggest a novel connection between slab-related arc mantle and geochemical signatures in some of the tholeiitic and mildly alkaline magmas of the Cretaceous High Arctic Large Igneous Province in the Sverdrup Basin. However, continental crustal contributions are noted in these evolved basaltic rocks. The integration of independent, yet complementary, data sets provides insight into present-day mantle structure, magmatic events, and relict oceans.

1. Introduction

The tectonic evolution of ocean basins can be deciphered from morphological and geophysical signatures preserved by oceanic crust and adjacent margins, including ophiolites, suture zones, and arc magmatism. Several decades of global data collection including magnetic and gravity anomalies provide key constraints for plate tectonic reconstructions and have been summarized and embedded in recent global models covering hundreds of millions of years [*Seton et al.*, 2012; *Domeier and Torsvik*, 2014]. However, in remote and complex regional tectonic settings dominated by several cycles of ocean basin opening and closure, such data are often spatially and temporally restricted and offer limited information about the geometry and timing of subducted oceanic lithosphere. Deciphering the tectonic evolution of continents and adjacent oceans in frontier regions such as the Arctic remains a challenge.

A large portion of the present Arctic Ocean is occupied by the Amerasia Basin (Figure 1), of which there is significant debate about the nature of its crust and timing of formation. Opening of the Amerasia Basin sometime during the Late Jurassic-Early Cretaceous [e.g., *Grantz et al.*, 2011; *Alvey et al.*, 2008] is considered to have been at the expense of subducting adjacent oceanic lithosphere (~1000 km wide) [e.g., *Nokleberg et al.*, 2000; *Sokolov et al.*, 2002; *Shephard et al.*, 2013]. In most regional reconstructions, the Amerasia Basin is formed by the rotation of Chukotka and the North Slope of Alaska (NSA; also referred to as the "Alaska-Chukotka microplate") away from the Canadian Arctic Islands (e.g., *Lawver et al.* [2002]; see review in *Shephard et al.* [2013]) though other mechanisms have been suggested [e.g., *Miller et al.*, 2010]. Geological evidence for a prior oceanic basin adjacent to northernmost Panthalassa includes the South Anuyi and Angayucham sutures (Figure 1), which run approximately from the New Siberian Islands to Alaska and are delineated by turbidites, ophiolites, granodiorites, and arc volcanic rocks [e.g., *Rowley and Lottes*, 1988; *Drachev et al.*, 1998].

An extinct Arctic Paleozoic-Mesozoic ocean, broadly located between the reconstructed NSA, Chukotka, and Kolyma/Siberia blocks, is often referred to as the South Anuyi-Angayucham Ocean (Figure 2). Regional subduction events during the Middle Jurassic-Early Cretaceous, include the Koyukuk, Oloy, and Nutesyn arcs, related to subduction and collision along the NSA, Kolyma-Omolon terrane, and Chukotka, respectively (Figure 2 and Figure S12 in the supporting information). The timing of final ocean closure along the suture (in at least the western regions) is given by a range of Early Cretaceous (pre-Albian) syncollisional and postcollisional dates including cross-cutting plutons (post-tectonic ~117 Ma) [*Miller et al.*, 2009; *Amato et al.*, 2015],

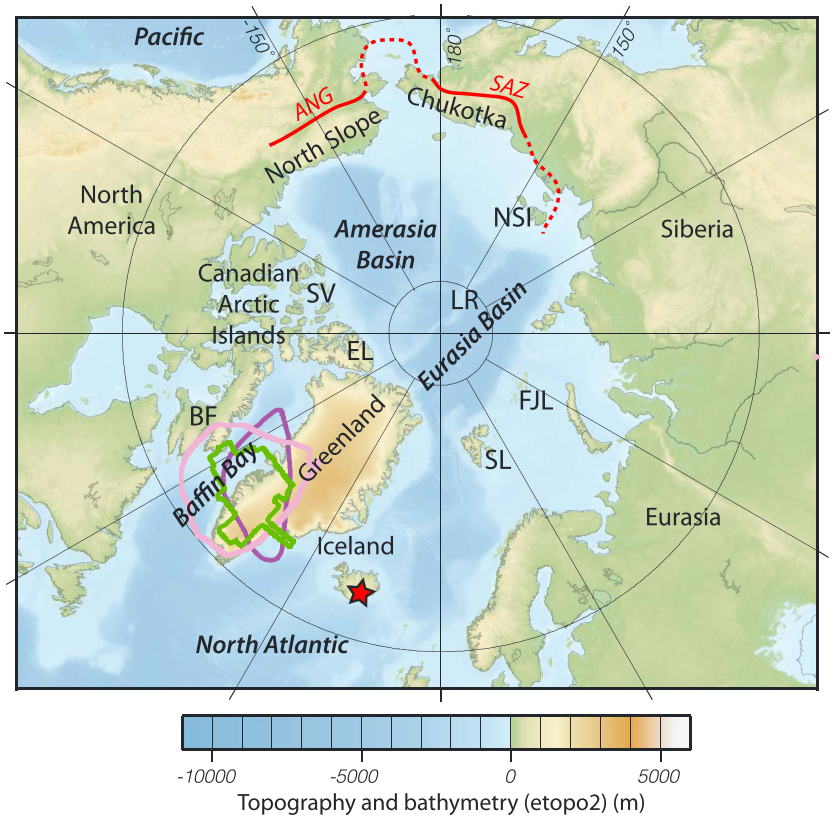

Figure 1. Overview of present Arctic Ocean region. BF: Baffin Island, EL: Ellesmere Island, FJL: Franz Josef Land, LR: Lomonosov Ridge, NSI: New Siberian Islands, SL: Svalbard, SV: Sverdrup Basin. Red line shows location of the Angayucham (ANG) and South Anuyi (SAZ) sutures, which are often linked, as indicated by the stippled lines [*Miller et al*., 2006]; red star: present-day Iceland hotspot. Purple/green lines are approximate Greenland slab extent around 1450 km (0.3% contour; dark purple: *S40RTS* [*Ritsema et al*., 2011], light purple: *GyPSuMS* [*Simmons et al*., 2010]; 0.15% contour, green: *UU-P07* [*Amaru*, 2007], Figure 3).

syncollisional sandstones (125 Ma maximum depositional age; *Amato et al*. [2015]; see also *Moore et al*. [2015] for summary of Brooks Range) and metamorphic domes (124–117 Ma) [*Toro et al*., 2003].

It is worth noting that alternative reconstructions to this singular ocean exist, whereby the NSA and Chukotka terranes are separate prior to Aptian (~125–113 Ma) times. These models reserve "South Anuyi" to the Chukotka-Kolyma/Siberia region and "Angayucham" to the NSA-adjacent area (Figure 2a) [*Amato et al*., 2015; *Till*, 2016]. This implies that the South Anuyi-Angayucham suture, while appearing linked at present day, is in fact two (or more) separate sutures. Regardless of one or more oceanic domains, Late Jurassic-Cretaceous subduction along the NSA (and often Chukotka), associated with its counterclockwise rotation and opening of the Amerasia Basin, is depicted in most tectonic models to date and represents the final stage of South Anuyi-Angayucham closure (Figure 2).

Ambiguity in published reconstructions and the generation of kinematically consistent and linked plate boundaries make a more detailed regional analysis beyond the scope of this study. Indeed, other ophiolite outcrops and sutures related to discrete episodes could be considered in reconstructing the South Anuyi-Angayucham history (e.g., Koyukuk arc and Kolyuchin-Mechigmen zone [*Till*, 2016]). Here we suggest that either Middle Jurassic-Cretaceous tectonic scenario, i.e., discrete spatial and/or temporal subduction episodes (approximately within 10–20 Myr, 500–1000 km), or a single ocean might account for the mantle slab structures discussed below. Notably, the size and robustness of the seismic anomaly under Greenland points to an ocean that was inboard from the main plates of Panthalassa and was likely separated by a long-lived offshore arc system [*Sigloch and Mihalynuk*, 2013; *Miller et al*., 2013]. For clarity we herein refer to this general area as the South Anuyi-Angayucham Ocean.

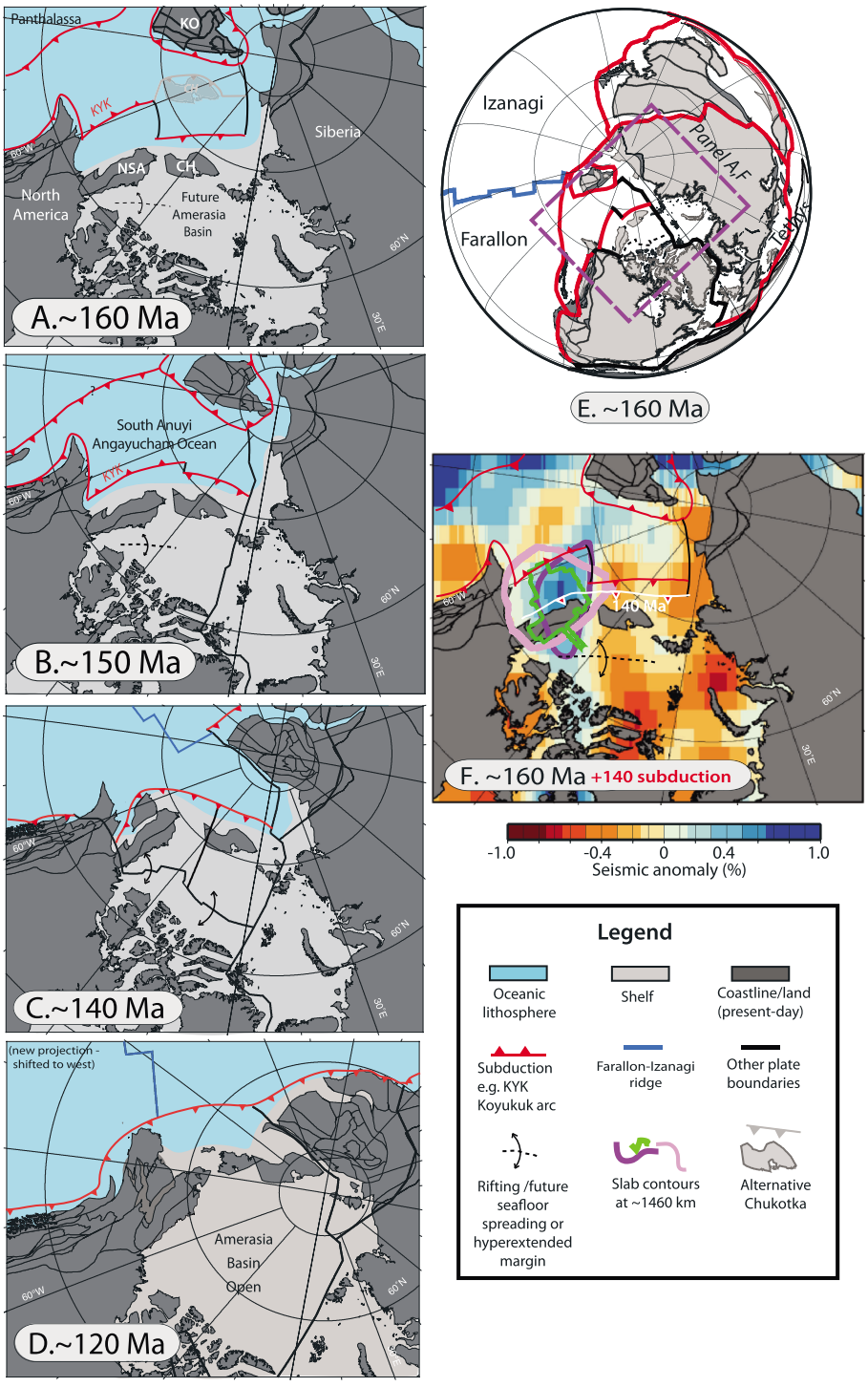

Figure 2. (a–d) Plate reconstructions at 160–120 Ma (adapted from *Shephard et al.* [2013]), around the onset of South Anuyi-Angayucham Ocean subduction, rotation of the North Slope and Chukotka, and opening of the Amerasia Basin. See inset legend for details. CH: Chukotka, KO: Kolyma-Omolon terrane, NSA: North Slope of Alaska. Light grey block and subduction at 160 Ma show approximate location of Chukotka in alternative models [e.g., *Amato et al.*, 2015] (Figure S12) and separation into two ocean basins. (e) Zoom-out showing Arctic in broader context at 160 Ma. (f) As in Figure 2a but underlain by seismic tomography model S40RTS (1460 km; contours as in Figures 1 and 3) showing Greenland slab in relation to overlying subduction zones, also at 140 Ma related to Amerasia Basin opening. Successive episodes of regional subduction with variable polarity and trench motion, rather than a singular event, may account for the seismic anomaly.

The incessant recycling of oceanic lithosphere by subduction means that only limited information about the age and structure of subducted oceans can be inferred from the few preserved sutures and ophiolitic complexes. Sparse or inaccessible outcrops and ambiguous paleomagnetic and geological data prove insufficient for recreating the detailed history of the South Anuyi-Angayucham Ocean; thus, complementary data sets and methods must be sought. One such approach is the joint analysis of regional tectonic data, kinematic plate models, and tomographic images, which not only integrate horizontal plate movements but also track subducted mantle material [e.g., *van der Meer et al*., 2010]. Following this approach, *Shephard et al*. [2013] mapped mantle provinces in tomographic models available for the Arctic and correlated them with specific subduction episodes. Among these regional positive velocity anomalies, one located ~1000–1600 km under present-day Greenland was noted. Based on a vertical correlation to paleosubduction zones, this mid-mantle anomaly was tentatively linked to paleo-Arctic subduction and, furthermore, could be broadly reproduced by coupled plate motion-mantle convection models [*Shephard et al*., 2014]. Here we explore available complementary evidence to support the existence of this distinct slab and evaluate its broader geodynamic implications over time.

2. Seismic Tomography

Seismic tomography models, based on *P* and/or *S* waves, image mantle anomalies which have relatively faster or slower velocities compared to depth-averaged mantle models. Faster anomalies are generally assigned to colder than ambient mantle material and are identified as subducted lithosphere. Efforts to link subduction history to surface kinematics using slabs imaged by seismic tomography have been undertaken on global [e.g., *van der Meer et al*., 2010, 2012] and regional scales [e.g., *Schellart and Spakman*, 2015] including the Arctic [*Shephard et al*., 2013; *Gaina et al*., 2014].

We focus on a distinct fast seismic feature in the mid-mantle, under present-day Greenland (Figure 1), visible in cross sections across several global tomography models (Figures 3 and S1–S3), including S40RTS [*Ritsema et al*., 2011], UU-P07 [*Amaru*, 2007], and GyPSuMS [*Simmons et al*., 2010] (*Grand* [2002] in the supporting information). The two models, S40RTS and UU-P07, are independent of each other and therefore are well suited to evaluate the robustness of a particular seismic anomaly of being an image of actual mantle structure. This Greenland anomaly ranges between ~1000 and 1600 km depth and has a peak in amplitude around 1400 km and an approximate center point of 50°W, 65°N (Table S1). A fast tomographic anomaly of unknown origin in the transition zone is imaged above this region, although not shared in all tomography models. We cannot exclude that part of the slab has stagnated (see sinking rate discussion for further analysis).

With model and depth-dependent variation, the anomaly is characterized by both subrounded and elongate geometries (Figure 3). Limited depth slices show a NW-SE elongation of the anomaly; however, considering its mid-mantle location, any relation to surface trench motions is not clear. The depth and location of the proposed slab from tomography are complicated by the subduction history, sinking behavior and associated advection and interaction with regional mantle flow. Nonetheless, the match between the mantle anomaly identified in tomography and surface kinematic reconstructions (i.e., absolute reference frame and assuming near vertical sinking) points to the South Anuyi-Angayucham Ocean.

The Greenland anomaly is separated from the deeper and prominent "Farallon slab," located farther west, by a region of negative (slow) seismic anomalies [e.g., *Grand et al*., 1997; *Sigloch et al*., 2008] (Figures 3, S1, and S2). The Farallon slab is considered to be related to subduction along North America from 100 Ma [*Grand et al*., 1997] or to intraoceanic subduction within northeast Panthalassa (Figure 2) [*Sigloch and Mihalynuk*, 2013]. The latter scenario might account for at least the northern portion of the Farallon slab which matches a long-lived Panthalassa subduction zone that existed far outboard of the South Anuyi-Angayucham Ocean (Figure 2). In combination with UU-P07 resolution tests (Figure S4; see *Hall and Spakman* [2015] for more information and quality assessment), this suggests a spatially separate and discrete subduction history for the Greenland anomaly and supports our paleo-Arctic interpretation. Other known Late Jurassic paleosubduction regions, namely, the Tethys, are too remote and could not account for the sub-Greenland slab. Improved resolution of both surface data sets and mantle tomography models may shed light on finer regional tectonic details.

3. Sinking Rates

To place the observed Greenland anomaly in a kinematic context, we explore a circum-Arctic plate reconstruction and assess the correlation between the age and depth of the inferred slab and the sinking rates.

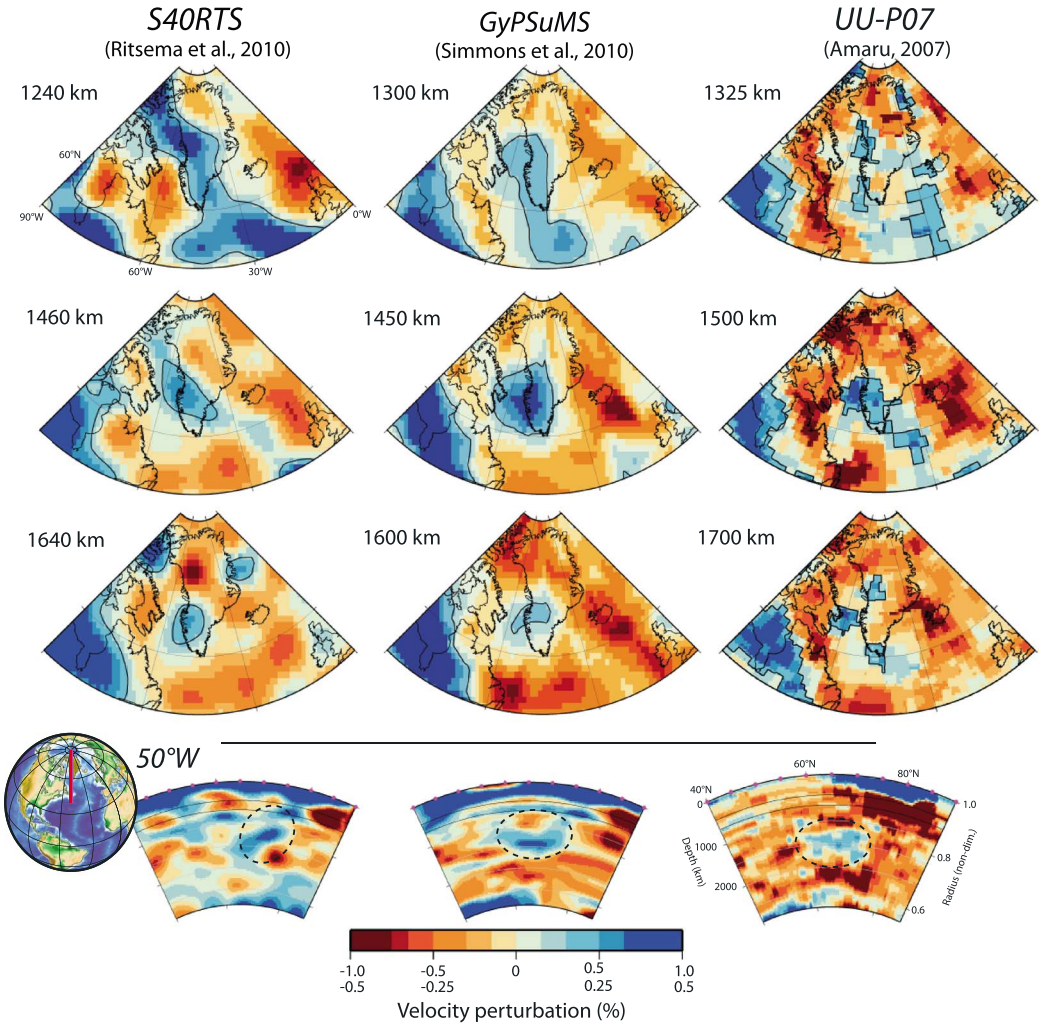

Figure 3. Horizontal slices ranging from ~1300 to 1600 km and vertical slices (50°W, 40–90°N, globe inset) through seismic tomography models S40RTS [*Ritsema et al*., 2011], GyPSuMS [*Simmons et al*., 2010], and UU-P07 [*Amaru*, 2007], half color scale due to model scaling. Black contour in horizontal slices identifies approximate slab edge based on the 0.3% seismic contour (0.15% UU-P07). Additional depths and *Grand* [2002] in Figures S1–S3.

In a fixed mantle frame, the mantle region under present-day Greenland was overlain by the Arctic and northernmost Panthalassa during the Mesozoic (Figure 2) [*Shephard et al*., 2013].

A dual sinking rate and slab subduction age approach (Table S2) is appropriate when the age of subduction is not well constrained by the geological record, as is the case in frontier regions such as the Arctic. Inferred sinking rates represent the averages of higher sinking rates in the low-viscosity upper mantle and transition zone, possible slab stagnation around 660 km and lower rates in the high-viscosity lower mantle [e.g., *Goes et al*., 2008; *Ricard et al*., 1993; *Steinberger and Calderwood*, 2006]. Notably, several recent studies present observational and experimental evidence for a strong viscosity gradient through the uppermost 300–500 km of the lower mantle, with a maximum at about 1000 km depth (800–1200 km) [*Fukao and Obayashi*, 2013; *Ballmer et al*., 2015; *French and Romanowicz*, 2015; *Marquardt and Miyagi*, 2015; *Rudolph et al*., 2015] (Figure 5c). Additional slab stagnation near the 660 km discontinuity may be due to endothermic transition from ringwoodite to a bridgemanite-dominated mineral assemblage and pyroxene and/or olivine metastability, especially in cold subduction zones [*King et al*., 2015; *Simmons et al*., 2015]. The high seismic velocity in the transition zone in two of the tomographic models (Figure 2) may explain slab remnants from the latest phase of subduction and supports our use of a globally averaged sinking rate.

Assuming vertical slab sinking and a slab base of 1600 km depth, a globally averaged sinking rate of 1.2 (±0.3) cm/yr [*van der Meer et al*., 2010; *Butterworth et al*., 2014] implies a subduction age at the trench of ~133 (range 177–106) Ma (Table S2). Conversely, applying a subduction age of 160 and 120 Ma to a 1600 km slab yields sinking rates of 1 and 1.3 cm/yr, respectively. This sinking rate/age estimate supports the known geological record of the South Anyui-Angayucham suture(s) and existence of an Arctic paleo-ocean. Final stages of South Anuyi-Angayucham Ocean subduction correlate with a Late Jurassic-Early Cretaceous timing of Amerasia Basin opening. Notably, slightly slower rates inferred by ~160 Ma subduction timing (e.g., 1 cm/yr for slab at 1600 km; Table S2) are still consistent with the estimates (1.2 ± 0.3 cm/yr) and concur with the recent observations of regional subduction in which slab rollback considerably slows down the overall sinking rate [*Simmons et al*., 2015]. Such a low rate may concur with the sinking of a relatively small slab volume (as imaged in tomography and based on the plate reconstruction), which may increase the thermal absorption and reduce the negative slab buoyancy and sinking speed. Furthermore, a significantly younger age of final South Anuyi-Angayucham subduction (younger than ~120 Ma), and consequently, a faster sinking rate conflicts with overriding location of the continents (i.e., no overriding oceans) at younger times, regardless of absolute reference frame (Figures 2 and S5 and Table S2).

4. Gravity Gradients

To further evaluate the existence of the Greenland anomaly, we investigate gravity gradient data from the GOCE (Gravity field and steady-state Ocean Circulation Explorer) satellite mission [*Johannessen et al*., 2003; *Rummel et al*., 2011]. Gravity gradients are highly sensitive to the geometry of anomalous bodies at depth, and we map the gravity vector variations in different directions. These second-order derivatives of the gravitational potential are thus well suited for elucidating longitudinally or latitudinally striking features such as slab remnants. Long-wavelength nonhydrostatic gravity gradient anomalies at satellite altitude (225–255 km) reflect 3-D mass heterogeneities within Earth's mantle and induced density interface deflections, including down to mid-mantle depths for a thin, vertically sinking slab, and to the deep mantle for wider mass anomalies [*Panet et al*., 2014]. At large scales, gradient anomalies coincide with regions of long-lived subduction and deep-seated convective instabilities/plumes [*Panet et al*., 2014]. The sign of the gradient anomalies changes with the source depth, and fine-scale oscillations can occur above the edges of the mass anomaly, if its width-to-depth ratio is high enough, which puts stronger constraints on the source than geoid or gravity anomaly data. Difficulties in scaling seismic velocity to density make this global gravity data set a valuable addition in deciphering mantle structure.

We present a regional analysis of these gravity gradients at intermediate wavelengths relevant for our purpose (Figure 4, 1300 and 1500 km; 800 km and additional directions, Figure S6). The coordinates (r, θ, and ϕ) are the usual spherical coordinates corresponding to the (e_r, e_θ, and e_φ) local frame, where e_r is pointing radially outward, e_θ is pointing toward the south, and e_φ toward the east. Direction "$\phi\phi$" is the second derivative in the E-W direction and reveals N-S trending anomalies, "$\theta\theta$" is second derivative in N-S direction highlighting E-W trending mass anomalies, respectively, while "*rr*" is the second derivative in the radial direction. We observe a negative gravity gradient anomaly in the $\phi\phi$ component, and $\theta\theta$ to a lesser extent, focused on Baffin Bay and southern Greenland, pointing to mass excess, as well as a positive (negative in "*rr*") anomaly on Baffin Island. Modeling results of a 1000 × 500 km cylindrical anomaly (density contrast 80 kg/m^3 relative to preliminary reference Earth model) between 1000 and 1500 km depth matches the magnitude and location of the gravity gradients, particularly for the $\phi\phi$ component (see supporting information, Figure S6, and Table S3). These gravity perturbations correspond with the slab location from tomography and provide additional support for a positive density anomaly under Greenland.

5. Possible Interactions With the High Arctic Large Igneous Province

The Cretaceous was a period of widespread Arctic magmatism identified in Franz Josef Land, Sverdrup Basin, De Long Islands, Svalbard, and North Greenland (Figures 1 and 5b, e.g., *Morgan* [1983] and *Tarduno et al*. [1998]). Often referred to as the High Arctic Large Igneous Province (HALIP), magmatism is thought to have formed in several stages ranging from ~130–80 Ma, although shorter-lived (~124–122 Ma) [*Corfu et al*., 2013] timings have been proposed for different locations. The origins of HALIP magmatism are unclear and possible links to deep mantle plumes (Figure 5) or global mantle overturn are tenuous [e.g., *Larson*, 1991;

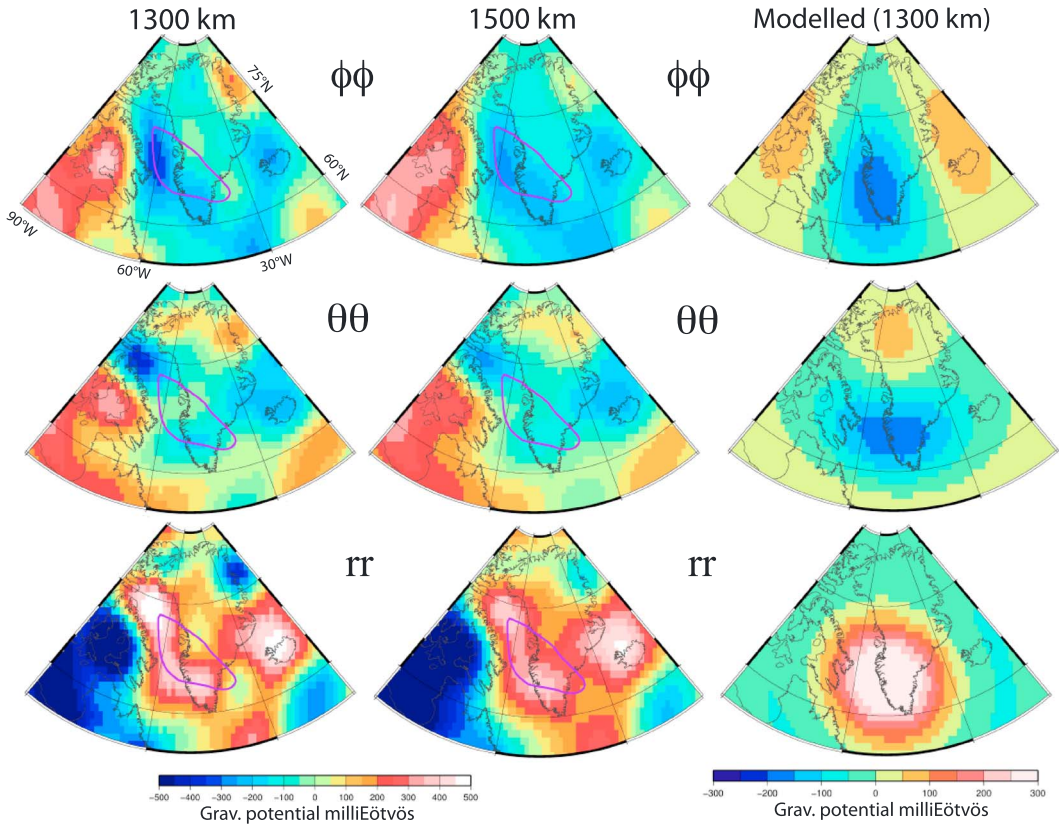

Figure 4. Gravity gradients [*Panet et al.*, 2014] filtered for 1300 and 1500 km wavelengths [*Panet et al.*, 2014] (800 km and additional directions in the supporting information and Figure S6), overlain with coastlines and S40RTS slab contour (Figure 2). Rightmost column shows forward-modeled gravity signal at the 1300 km wavelength (500 × 1000 km cylinder, 80 kg/m^3 density contrast). Gravity directions $\phi\phi$, $\theta\theta$, and *rr* highlight mantle mass features which show N-S, E-W, and radial variations, respectively.

Lawver and Müller, 1994; *Smirnov and Tarduno*, 2000]. Although the temporally and spatially overlapping events of Amerasia Basin opening, South Anuyi-Angayucham subduction and HALIP eruption appear related; geodynamic and geochemical relationships between them have not been established.

Geochemically characterized HALIP basaltic rocks from the Sverdrup Basin include 130–80 Ma tholeiitic rocks at Ellef Ringnes and Axel Heiberg islands and 85–60 Ma mildly alkaline basaltic rocks at Ellesmere Island [*Estrada*, 2014; *Evenchick et al.*, 2015; *Jowitt et al.*, 2014]. Franz Josef Land (FJL) basalts are also tholeiitic [*Ntaflos and Richter*, 2003] and generally more primitive than the basaltic rocks of the Sverdrup Basin.

Paleogeographic reconstructions of the Sverdrup Basin, combined with the imaged sub-Greenland slab and inferred subduction zone positions (Figures 2, 5, and S5), indicate that the HALIP melting region under the Sverdrup Basin at about 120 Ma may have coincided with the arc and back-arc mantle related to ~160–120 Ma South Anuyi-Angayucham subduction. Suprasubduction asthenosphere affected by the infiltration of fluids and melts from the breakdown of hydrous minerals and carbonates will acquire chemical signatures characteristic of many of the Sverdrup Basin HALIP basaltic rocks, especially the tholeiites from Ellef Ringnes and Axel Heiberg islands. These signatures include the elevated ratios of Pb/(Ce + Pr), Rb/Ba, and (Th + U)/(Nb + Ta) observed in normalized trace element diagrams (spider diagrams Figure 5a).

A preexisting arc or back-arc mantle from South Anuyi-Angayucham subduction could partly mix with and contaminate material supplied by a deep plume-type upwelling before or during shallow asthenospheric melting, resulting in the HALIP magmas. An average of samples from Heimaey in the Southern Volcanic Flank Zone of Iceland is included in Figure 5a as an example of a deep plume source with a considerable proportion of recycled oceanic crust (ROC). In contrast to the enriched tholeiitic rocks from Ellef Ringnes and Axel Heiberg islands, the Heimaey basalts are characterized by low ratios of Pb/(Ce + Pr), Rb/Ba, and (Th + U)/(Nb + Ta), as well

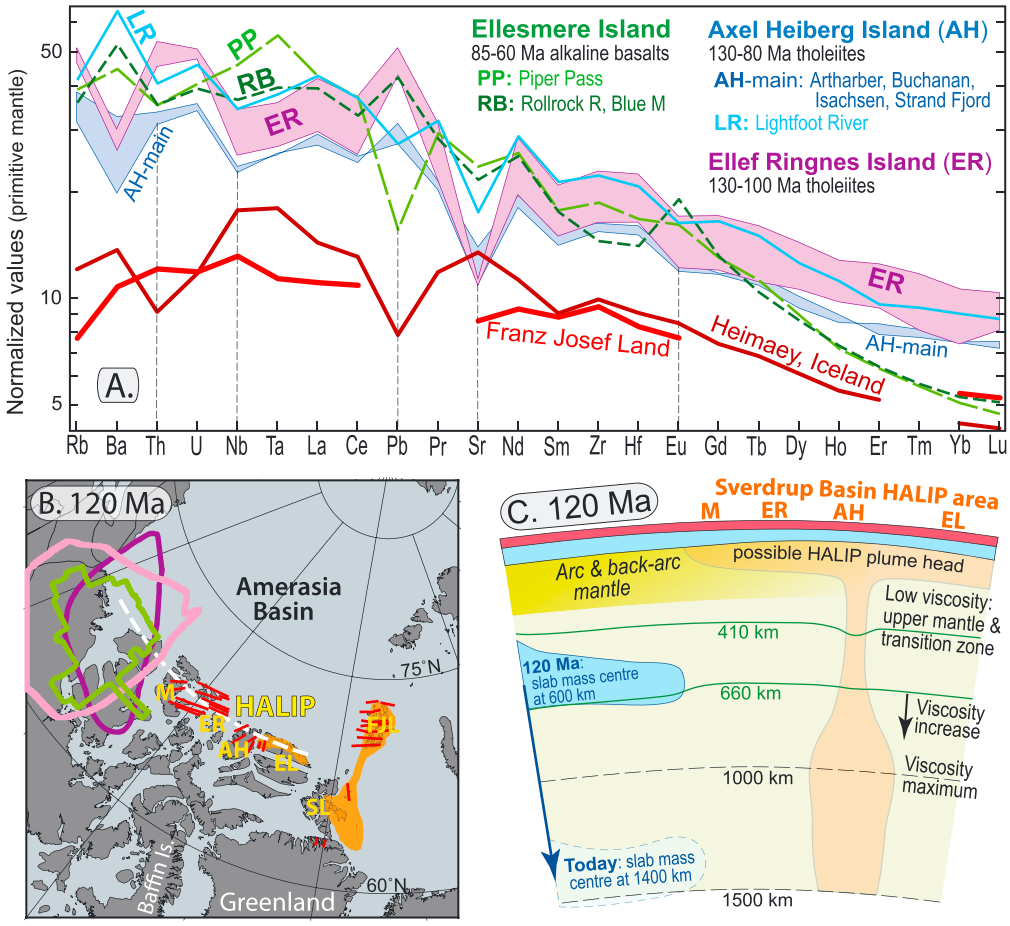

Figure 5. (a) Trace element concentrations normalized to primitive mantle [*Sun and McDonough*, 1989] for HALIP basaltic rocks from Ellef Ringnes [*Evenchick et al.*, 2015], Ellesmere and Axel Heiberg islands [*Jowitt et al.*, 2014; *Estrada*, 2014], and Franz Josef Land [*Ntaflos and Richter*, 2003]. The fields and lines representing the HALIP units are averages and ranges specified in Figures S7–S9. Samples from the Vestmanaeyjar system (Heimaey, Iceland) with a strong recycled oceanic lithosphere signature are included for comparison [*Peate et al.*, 2010]. After removal of the evolved and fractionated samples with <4.5 wt % MgO, the rocks from the same formations and areas were grouped and averaged (supporting information). (b) ~ 120 Ma plate reconstruction, coeval with major HALIP activity at Ellef Ringnes and Axel Heiberg Island. Dykes and volcanic regions are in red and orange. AH, EL, ER, and M: Axel Heiberg, Ellesmere, Ellef Ringnes, and Melville islands, respectively; FJL: Franz Josef Land; SL: Svalbard. Purple/green lines show the approximate slab extent (Figure 1), thick white line is trace of vertical section C. (c) Schematic model at 120 Ma. The arc and back-arc mantle affected by supra-subduction fluid and melt infiltration processes, and a possible HALIP-related plume is indicated.

as lower concentrations of most of the trace elements. In spite of incomplete data coverage, the HALIP basalts from FJL appear to be relatively similar to, and even less enriched than the Heimaey basalts. Based on the trace element patterns, arc or back-arc mantle contributions to the FJL basalts are therefore unlikely. The 120 Ma paleogeographic reconstructions and the schematic vertical section (Figures 2, 5b, and 5c) supports the notion that the 130–80 Ma tholeiitic rocks at Ellef Ringnes and Axel Heiberg islands are most likely to be affected by arc and back-arc mantle sources.

The elevated Sr/(Pr + Nd) ratios in the Heimaey basalts compared to all of the HALIP rocks in Figure 5a is due to assimilation of some gabbroic rocks from the thick and young oceanic basement crust generated in the Icelandic rift zone. The opposite process of plagioclase fractionation can explain the common Sr depletion in the HALIP basaltic rocks and in many other evolved basaltic suites.

Unfortunately, the arc-type chemical signature of most of the tholeiites from Ellef Ringnes and Axel Heiberg is not unambiguous and could potentially be related to contamination with upper continental crust (UCC). Considerable amounts of UCC contamination, however, are likely to impose heterogeneities between and

within individual magma batches. A more complete discussion of the chemical variability of the HALIP basalts and the possibilities of UCC contamination is provided as supporting information.

In summary, geochemical features indicate that several of the 130–80 Ma tholeiitic rocks from Ellef Ringnes and Axel Heiberg islands, which at eruption times were closest to the former South Anuyi-Angayucham subduction, may have incorporated significant amounts of arc and back-arc mantle. Although a clear discrimination between arc-like mantle sources and upper crustal contamination is difficult, we find that some of the distinct trace element concentration patterns across the different volcanic and subvolcanic units may have resulted from arc-like mantle sources associated with the South Anuyi-Angayucham slab(s). Trace element patterns in the HALIP basalts in the Sverdrup Basin suggest that suprasubduction, arc-type mantle might have mixed with plume-supplied material.

6. Conclusions

Independent *P* and *S* wave tomography models image a distinct, mid-mantle (1000–1600 km) positive seismic anomaly under present-day Greenland, which is spatially linked to perturbations in gravity gradients. We interpret the mantle anomaly as a remnant of subduction. Using plate reconstructions in a mantle reference frame and assuming vertical slab sinking, we link the position of this anomaly to the closure of the South Anuyi-Angayucham Ocean. Final stages of regional subduction were likely linked to the complementary opening of the Amerasia Basin. Consistent with a range of whole-mantle sinking rates (1.2 ± 0.3 cm/yr) and evidence from the geological record, the slabs were likely subducted in the Late Jurassic-Early Cretaceous. Although minor crustal contamination is likely, HALIP geochemistry in the Sverdrup Basin seems to incorporate arc-mantle sources, bringing the origin of the HALIP a step further to resolution. The combination of seismic tomography, satellite gravimetry, and plate reconstructions shed new light on the mantle evolution under present-day Greenland.

Acknowledgments

G.E.S., R.G.T., W.S., and C.G. acknowledge support from the Research Council of Norway through its Centres of Excellence funding scheme, project 22372. I.P. acknowledges CNES for financial support through the TOSCA committee. Data supporting the conclusions can also be obtained in the supporting information. We thank Marianne Greff-Lefftz for computing the gravity modeling. We would like to thank the Editor Michael Wysession, as well as Nathan Simmons and an anonymous reviewer for their helpful comments that improved the manuscript. We also thank Elizabeth Miller for advice on an earlier version of the manuscript.

References

Alvey, A., C. Gaina, N. J. Kusznir, and T. H. Torsvik (2008), Integrated crustal thickness mapping and plate reconstructions for the high Arctic, *Earth Planet. Sci. Lett.*, *274*(3–4), 310–321.

Amaru, M. L. (2007), Global travel time tomography with 3-D reference models, *Geol. Ultraiectina*, *274*, 174.

Amato, J. M., J. Toro, V. V. Akinin, B. A. Hampton, A. S. Salnikov, and M. I. Tuchkova (2015), Tectonic evolution of the Mesozoic South Anyui suture zone, eastern Russia: A critical component of paleogeographic reconstructions of the Arctic region, *Geosphere*, *11*(5), 1530, doi:10.1130/GES01165.1.

Ballmer, M. D., N. C. Schmerr, T. Nakagawa, and J. Ritsema (2015), Compositional mantle layering revealed by slab stagnation at ~1000-km depth, *Sci. Adv.*, *1*, e1500815.

Butterworth, N. P., A. S. Talsma, R. D. Müller, M. Seton, H.-P. Bunge, B. S. A. Schuberth, G. E. Shephard, and C. Heine (2014), Geological, tomographic, kinematic and geodynamic constraints on the dynamics of sinking slabs, *J. Geodyn.*, *73*, 1–13.

Corfu, F., S. Polteau, S. Planke, J. I. Faliede, H. Svenson, A. Zayoncheck, and N. Stolbov (2013), U-Pb geochronology of Cretaceous magmatism on Svalbard and Franz Josef Land, Barents Sea Large Igneous Province, *Geol. Mag.*, *150*(06), 1127–1135.

Domeier, M., and T. H. Torsvik (2014), Plate tectonics in the late Paleozoic, *Geosci. Front.*, *5*(3), 303–350.

Drachev, S. S., L. A. Savostin, V. G. Groshev, and I. E. Bruni (1998), Structure and geology of the continental shelf of the Laptev Sea, Eastern Russian Arctic, *Tectonophysics*, *298*(4), 357–393.

Estrada, S. (2014), Geochemical and Sr–Nd isotope variations within Cretaceous continental flood-basalt suites of the Canadian High Arctic, with a focus on the Hassel Formation basalts of northeast Ellesmere Island, *Int. J. Earth Sci.*, doi:10.1007/s00531-014-1066-x.

Evenchick, C. A., W. J. Davis, J. H. Bédard, N. Hayward, and R. M. Friedman (2015), Evidence for protracted High Arctic large igneous province magmatism in the central Sverdrup Basin from stratigraphy, geochronology, and paleodepths of saucer-shaped sills, *Geol. Soc. Am. Bull.*, *127*, 1366.

French, S. W., and B. Romanowicz (2015), Broad plumes rooted at the base of the Earth's mantle beneath major hotspots, *Nature*, *525*, 95–99.

Fukao, Y., and M. Obayashi (2013), Subducted slabs stagnant above, penetrating through, and trapped below the 660 km discontinuity, *J. Geophys. Res. Solid Earth*, *118*, 5920–5938, doi:10.1002/2013JB010466.

Gaina, C., S. Medvedev, T. Torsvik, I. Koulakov, and S. Werner (2014), 4D Arctic: A glimpse into the structure and evolution of the Arctic in the light of new geophysical maps, plate tectonics and tomographic models, *Surv. Geophys.*, *35*(5), 1095–1122.

Goes, S., F. A. Capitanio, and G. Morra (2008), Evidence of lower-mantle slab penetration phases in plate motions, *Nature*, *451*, 981–984.

Grand, S. P. (2002), Mantle shear-wave tomography and the fate of subducted slabs, *Philos. Trans. R. Soc. A*, *360*, 2475–2491.

Grand, S. P., R. D. van der Hilst, and S. Widiyantoro (1997), Global seismic tomography: A snapshot of convection in the Earth, *GSA Today*, *7*(4), 1–7.

Grantz, A., P. E. Hart, and V. A. Childers (2011), Chapter 50: Geology and tectonic development of the Amerasia and Canada Basins, Arctic Ocean, *Geol. Soc. London Mem.*, *35*(1), 771–799.

Hall, R., and W. Spakman (2015), Mantle structure and tectonic history of SE Asia, *Tectonophysics*, *658*, 14–45.

Johannessen, J. A., et al. (2003), The European Gravity Field and steady-state Ocean Circulation Explorer satellite mission its impact on geophysics, *Surv. Geophys.*, *24*(4), 339–386.

Jowitt, S. M., M.-C. Williamson, and R. E. Ernst (2014), Geochemistry of the 130 to 80 Ma Canadian High Arctic Large Igneous Province (HALIP) event and implications for Ni-Cu-PGE prospectivity, *Econ. Geol.*, *109*(2), 281–307.

King, S. D., D. J. Frost, and D. C. Rubie (2015), Why cold slabs stagnate in the transition zone, *Geology*, *43*, 231–234.

Larson, R. L. (1991), Geological consequences of superplumes, *Geology*, *19*, 963–966.
Lawver, L. A., and R. D. Müller (1994), Iceland hotspot track, *Geology*, *22*(4), 311–314.
Lawver, L. A., A. Grantz, and L. M. Gahagan (2002), Plate kinematic evolution of the present Arctic region since the Ordovician, in *Tectonic Evolution of the Bering Shelf–Chukchi Sea–Arctic Margin and Adjacent Landmasses*, edited by E. L. Miller, A. Grantz, and S. L. Klemperer, *Geol. Soc. Am. Spec. Pap.*, *360*, 333–358.
Marquardt, H., and L. Miyagi (2015), Slab stagnation in the shallow lower mantle linked to an increase in mantle viscosity, *Nat. Geosci.*, *8*, 311–314.
Miller, E. L., J. Toro, G. Gehrels, J. M. Amato, A. Prokopiev, M. I. Tuchkova, V. V. Akinin, T. A. Dumitru, T. E. Moore, and M. P. Cecile (2006), New insights into Arctic paleogeography and tectonics from U-Pb detrital zircon geochronology, *Tectonics*, *25*, TC3013, doi:10.1029/2005TC001830.
Miller, E. L., S. M. Katkov, A. Strickland, J. Toro, V. Akinin, and T. A. Dumitru (2009), Geochronology and thermochronology of Cretaceous plutons and metamorphic country rocks, Anyui-Chukotka fold belt, northeastern Arctic Russia, in *Geology, Geophysics and Tectonics of Northeastern Russia: A Tribute to Leonid Parfenov*, *Stephan Mueller Spec. Publ. Ser.*, vol. 4, edited by D. B. Stone et al., pp. 223–241, European Geophysical Union, Copernicus GmbH, Göttingen Germany.
Miller, E. L., G. Gehrels, V. Pease, and S. Sokolov (2010), Stratigraphy and U-Pb detrital zircon geochronology of Wrangel Island, Russia: Implications for Arctic paleogeography, *AAPG Bull.*, *94*(5), 665–692.
Miller, E. L., A. V. Soloviev, A. Prokopiev, J. Toro, D. Harris, A. B. Kuzmichev, and G. E. Gehrels (2013), Triassic river systems and the paleo-Pacific margin of northwestern Pangea, *Gondwana Res.*, *23*, 1631–1645.
Moore, T. E., P. B. O'Sullivan, C. J. Potter, and R. A. Donelick (2015), Provenance and detrital zircon geochronologic evolution of lower Brookian foreland basin deposits for the western Brooks Range, Alaska, and implications for early Brookian tectonics, *Geosphere*, *11*(1), 1–30.
Morgan, W. J. (1983), Hotspot tracks and the early rifting of the Atlantic, in *Developments in Geotectonics*, edited by P. Morgan and B. H. Baker, pp. 123–139, Elsevier, Amsterdam.
Nokleberg, W. J., L. M. Parfenov, J. W. H. Monger, I. O. Norton, A. I. Khanchuk, D. B. Stone, C. R. Scotese, D. W. Scholl, and K. Fujita (2000), Phanerozoic tectonic evolution of the circum-North Pacific, Professional Paper, 1626, 122 pp., *U.S. Geol. Surv*, *Washington*, *D. C.*
Ntaflos, T., and W. Richter (2003), Geochemical constraints on the origin of the continental flood basalt magmatism in Franz Josef Land, Arctic Russia, *Eur. J. Mineral.*, *15*(4), 649–663.
Panet, I., G. Pajot-Metivier, M. Greff-Lefftz, L. Metivier, M. Diament, and M. Mandea (2014), Mapping the mass distribution of Earth's mantle using satellite-derived gravity gradients, *Nat. Geosci.*, *7*(2), 131–135.
Peate, D. W., K. Breddam, J. A. Baker, M. D. Kurz, A. K. Barker, T. Prestvik, N. Grassineau, and A. C. Skovgaard (2010), Compositional characteristics and spatial distribution of enriched Icelandic mantle components, *J. Petrol.*, *51*(7), 1447–1475.
Ricard, Y., M. Richards, C. Lithgow-Bertelloni, and Y. Le Stunff (1993), A geodynamic model of mantle density heterogeneity, *J. Geophys. Res.*, *98*(B12), 21,895–21,909, doi:10.1029/93JB02216.
Ritsema, J., A. Deuss, H. J. van Heijst, and J. H. Woodhouse (2011), S40RTS: A degree-40 shear-velocity model for the mantle from new Rayleigh wave dispersion, teleseismic traveltime and normal-mode splitting function measurements, *Geophys. J. Int.*, *184*(3), 1223–1236.
Rowley, D. B., and A. L. Lottes (1988), Plate-kinematic reconstructions of the North Atlantic and Arctic: Late Jurassic to present, *Tectonophysics*, *155*(1–4), 73–120.
Rudolph, M. L., V. Lekic, and C. Lithgow-Bertelloni (2015), Viscosity jump in Earth's mid-mantle, *Science*, *350*, 1349–1352.
Rummel, R., W. Yi, and C. Stummer (2011), GOCE gravitational gradiometry, *J. Geod.*, *85*(11), 777–790.
Schellart, W. P., and W. Spakman (2015), Australian plate motion and topography linked to fossil New Guinea slab below Lake Eyre, *Earth Planet. Sci. Lett.*, *421*, 107–116.
Seton, M., et al. (2012), Global continental and ocean basin reconstructions since 200 Ma, *Earth Sci. Rev.*, *113*(3–4), 212–270.
Shephard, G. E., R. D. Müller, and M. Seton (2013), The tectonic evolution of the Arctic since Pangea breakup: Integrating constraints from surface geology and geophysics with mantle structure, *Earth Sci. Rev.*, *124*, 148–183.
Shephard, G. E., N. Flament, S. Williams, M. Seton, M. Gurnis, and R. D. Müller (2014), Circum-Arctic mantle structure and long-wavelength topography since the Jurassic, *J. Geophys. Res. Solid Earth*, *119*, 7889–7908, doi:10.1002/2014JB011078.
Sigloch, K., and M. G. Mihalynuk (2013), Intra-oceanic subduction shaped the assembly of Cordilleran North America, *Nature*, *496*(7443), 50–56.
Sigloch, K., N. McQuarrie, and G. Nolet (2008), Two-stage subduction history under North America inferred from multiple-frequency tomography, *Nat. Geosci.*, *1*(7), 458–462.
Simmons, N. A., A. M. Forte, L. Boschi, and S. P. Grand (2010), GyPSuM: A joint tomographic model of mantle density and seismic wave speeds, *J. Geophys. Res.*, *115*, B12310, doi:10.1029/2010JB007631.
Simmons, N. A., C. S. Myers, G. Johannesson, E. Mazel, and S. P. Grand (2015), Evidence for long-lived subduction of an ancient tectonic plate beneath the southern Indian Ocean, *Geophys. Res. Lett.*, *42*, 9270–9278, doi:10.1002/2015GL066237.
Smirnov, A. V., and J. A. Tarduno (2000), Low-temperature magnetic properties of pelagic sediments (Ocean Drilling Program Site 805C): Tracers of maghemitization and magnetic mineral reduction, *J. Geophys. Res.*, *105*(B7), 16,457–16,471, doi:10.1029/2000JB900140.
Sokolov, S. D., G. Y. Bondarenko, O. L. Morozov, V. A. Shekhovtsov, S. P. Glotov, A. V. Ganelin, and I. R. Kravchenko-Berezhnoy (2002), South Anyui suture, northeast Arctic Russia: Facts and problems, *Geol. Soc. Am. Spec. Pap.*, *360*, 209–224.
Steinberger, B., and A. R. Calderwood (2006), Models of large-scale viscous flow in the Earth's mantle with constraints from mineral physics and surface observations, *Geophys. J. Int.*, *167*(3), 1461–1481.
Sun, S.-S., and W. F. McDonough (1989), Chemical and isotopic systematics of oceanic basalts: Implications for mantle composition and processes, *Geol. Soc. London Spec. Publ.*, *42*(1), 313–345.
Tarduno, J. A., D. B. Brinkman, P. R. Renne, R. D. Cottrell, H. Scher, and P. Castillo (1998), Evidence for extreme climatic warmth from Late Cretaceous Arctic vertebrates, *Science*, *282*(5397), 2241–2243.
Till, A. B. (2016), A synthesis of Jurassic and Early Cretaceous crustal evolution along the southern margin of the Arctic Alaska-Chukotka microplate and implications for defining tectonic boundaries active during opening of Arctic Ocean basins, *Lithosphere, Geol. Soc. Am.*, doi:10.1130/L471.1.
Toro, J., J. M. Amato, and B. Natal'in (2003), Cretaceous deformation, Chegitun River area, Chukotka Peninsula, Russia: Implications for the tectonic evolution of the Bering Strait region, *Tectonics*, *22*(3), 1021, doi:10.1029/2001TC001333.
van der Meer, D. G., W. Spakman, D. J. J. van Hinsbergen, M. L. Amaru, and T. H. Torsvik (2010), Towards absolute plate motions constrained by lower-mantle slab remnants, *Nat. Geosci.*, *3*(1), 36–40.
van der Meer, D. G., T. H. Torsvik, W. Spakman, D. J. J. van Hinsbergen, and M. L. Amaru (2012), Intra-Panthalassa Ocean subduction zones revealed by fossil arcs and mantle structure, *Nat. Geosci.*, *5*(3), 215–219.